Research Square

Preprints are preliminary reports that have not undergone peer review.
They should not be considered conclusive, used to inform clinical practice,
or referenced by the media as validated information.

Disentangling extraction and tidal effects on Sentinel-2 shoreline change rates: pixel-based versus sub-pixel shorelines along the Da Nang coast, Vietnam

Diem Phung Thi My

Ho Chi Minh City University of Natural Resources and Environment, 236B Le Van Sy Street, Tan Son Hoa Ward

Nga Duong Thi Thuy

dttnga_cntt@hcmunre.edu.vn

Ho Chi Minh City University of Natural Resources and Environment, 236B Le Van Sy Street, Tan Son Hoa Ward

Research Article

Keywords: Coastal setback zone, Coastal erosion management, Satellite-derived shoreline, Sub-pixel extraction, Sentinel-2, Tide correction

Posted Date: November 26th, 2026

DOI: https://doi.org/10.21203/rs.3.rs-11660424/v1

License: This work is licensed under a Creative Commons Attribution 4.0 International License.
Read Full License

Additional Declarations: No competing interests reported.

Disentangling extraction and tidal effects on Sentinel-2 shoreline change rates: pixel-based versus sub-pixel shorelines along the Da Nang coast, Vietnam

Abstract

Satellite-derived shorelines analysed with the Digital Shoreline Analysis System (DSAS) underpin many erosion assessments, yet the effects of extraction method, tidal stage and image selection are rarely compared on one dataset. This study quantifies all three on the Da Nang coast, Vietnam, using pixel-based (thresholded modified normalised difference water index) and sub-pixel (Shoreline Analysis and Extraction Tool) shorelines extracted from 11 Sentinel-2 scenes (2016 - 2026) and compared on 1,914 transects. Agreement was assessed with Bland–Altman analysis, weighted kappa and block bootstrapping; rates were recomputed for all date subsets spanning at least 8 years, and FES2022 tide corrections were tested over beach slopes of 0.03 - 0.12. Pixel-based shorelines lay 4.8 - 7.6 m seaward of sub-pixel shorelines, although offsets at one transect correlated weakly between dates (mean $r = 0.24$). Linear regression rates agreed closely ($r = 0.990$; bias - 0.07 m yr^{-1}; limits of agreement - 0.84 to + 0.70 m yr^{-1}). Tide correction raised the mean rate by 0.11 - 0.45 m yr^{-1}, and three-date subsets gave coast-mean rates from - 0.60 to +1.48 m yr^{-1}; the 2016 – 2020 - 2025 subset indicated net retreat, whereas all 11 dates gave + 0.57 m yr^{-1}. Without independent reference shorelines, these results describe agreement rather than accuracy. Extraction method mattered less than which images entered the analysis, so assessments based on few dates should report the sensitivity of rates to date selection and tide.

Keywords Shoreline change · Sentinel-2 · Sub-pixel extraction · DSAS · Tide correction · Uncertainty

1 Introduction

Shoreline position, and the way it shifts over years to decades, is among the most widely used indicators in coastal management. Rates of shoreline change feed directly into erosion hazard assessments, the delineation of coastal setback zones and the design of protection works (Boak and Turner 2005; Mentaschi et al. 2018; Vousdoukas et al. 2020). Since the Landsat and Sentinel-2 archives became freely available, shorelines can be mapped repeatedly over long coastlines at little cost, and satellite-derived shorelines (SDS) are now routinely processed with the Digital Shoreline Analysis System (DSAS) to obtain end-point and regression rates (Attwan, Alboabidalah, and Al-Zuhairy 2026; Chen et al. 2026; Himmelstoss et al. 2018, 2021; Luijendijk et al. 2018; Sun et al. 2023; Trinh et al. 2026; Yadav, Dodamani, and Dwarakish 2021).

Such rates can be no more reliable than the shoreline positions from which they are computed. Most applied studies still rely on pixel-based extraction, in which a water index such as the normalised difference water index (NDWI), the modified NDWI (MNDWI) or the automated water extraction index (AWEI) is thresholded and the boundary between the water and land classes is taken as the shoreline (Amoroso, Figliomeni, and Parente 2023; Dervisoglu, Bilgilioğlu, and Yağmur 2019; Xu 2006; Yulianto et al. 2022). The line obtained in this way follows the pixel grid, and its position depends on the chosen threshold and on how mixed pixels, swash foam and turbid nearshore water are classified (Bergsma et al. 2024; Yulianto et al. 2022). Sub-pixel methods were proposed to relax this constraint: rather than classifying pixels, they model the radiometric transition across the land - water interface and place the shoreline within the boundary pixel (Bishop-Taylor et al. 2019; Pardo-Pascual et al. 2012). The Shoreline Analysis and Extraction Tool (SAET) implements this approach for Sentinel-2 and Landsat

imagery, and assessments on sandy beaches have reported horizontal errors comparable to, or smaller than, the pixel size (Cabezas-Rabadán et al. 2025; Palomar-Vázquez et al. 2023; Vos et al. 2023).

Extraction is not, however, the only source of error in satellite-derived rates, because an SDS is an instantaneous waterline whose cross-shore position also reflects the tide, wave set-up and run-up at the time of acquisition, scaled by the slope of the intertidal beach (Castelle et al. 2021). On a beach with a slope of 0.05, a water-level difference of only 0.2 m between two images moves the waterline by about 4 m, which is of the same order as the accuracy reported for sub-pixel algorithms. Tidal corrections were long considered impractical in regions without tide gauges or beach surveys, but global tide models and beach slopes retrieved from SDS time series now make them feasible without field data (Lyard et al. 2021; Vos et al. 2020; Vos, Splinter, et al. 2019).

A third factor receives less attention in applied work: which images enter the calculation. Shoreline position varies from month to month and from year to year, and satellite records resolve that variability on sandy coasts (Vos, Harley, et al. 2019). End-point rates use only two shorelines, and most rate methods treat departures from a linear trend as noise (Genz et al. 2007). Many regional assessments nevertheless rest on a handful of dates, so a rate may depend on the particular images retained. How large this dependence is, relative to the choice of extraction method, can be tested directly when several dates are processed with both methods.

Comparisons between extraction methods are usually reported as the distance separating the two shorelines, often as an unsigned point-to-line distance. Unsigned distances hide whether one method consistently places the shoreline further seaward, and they say nothing about whether the separation persists from one date to the next, which is what decides whether it reaches the rate. To our knowledge, the transfer of inter-method offsets into DSAS rates has not been weighed against the effects of tide and date selection on one multi-year dataset.

The Da Nang coast in central Vietnam is well suited to this question. It is a microtidal, wave-dominated coast on which long sandy beaches alternate with the rocky Son Tra headland and the Cua Dai inlet of the Thu Bon River, and where rapid tourism and urban growth have increased the demand for dependable erosion information. DSAS has been applied extensively along the Vietnamese coast (Lappe, Ullmann, and Bachofer 2022; Nguyen and Hens 2017; Nguyen et al. 2017), and shoreline change in this sector has been documented with DSAS and CoastSat, in part to support the definition of coastal setback zones (Dinh et al. 2021; Ngo et al. 2020; Nguyen, Tran, and Trieu 2025). These studies relied on a single extraction method and did not quantify how much of the reported change could be attributed to extraction, tide or image selection (**Table 1**).

Table 1 Previous shoreline-change studies on the Da Nang – Quang Nam coast compared with this study

Study	Coast section	Imagery and period	Extraction method	Tide correction	Uncertainty assessed
Ngo et al. (2020)	Son Tra – Cua Dai	1965 topographic map (1:50,000); Landsat MSS/TM/ETM+ (1973, 1990, 2001); 30 VHR Google Earth images (2002–2019); 34 shorelines	Manual digitising (map, VHR); NDWI (1973) and MNDWI (1990, 2001), pixel-based	Not applied	Partly: a priori interpretation uncertainty per source (3.7–60 m) used in WLR/EPRunc; no independent validation
Dinh et al. (2021)	Quang Nam	All Landsat 4–5/7/8 and Sentinel-2 scenes (< 20% cloud), 1990–2019; 7 annual shorelines	mNDWI, zero threshold; annual Water Frequency Index composites (pixel-based)	Not applied; short-term water-level effects reduced by annual compositing	Not quantified; positional uncertainty inferred from observation count (<1 m for ≥30 scenes, after Xu)

Study	Coast section	Imagery and period	Extraction method	Tide correction	Uncertainty assessed
Nguyen et al. (2025)	Da Nang	Landsat 5/7/8/9 and Sentinel-2, 2004–2024	CoastSat (sub-pixel)	Applied (tide source and beach slope not reported)	RMSE ±10–15 m (Landsat), ±5–7 m (S2); reference data not specified
This study	Son Tra – Tam Hai	Sentinel-2, 11 scenes, 2016–2026	MNDWI and SAET	FES2022, sensitivity	Yes: inter-method agreement (Bland–Altman, weighted κ), date selection, tidal sensitivity, regression confidence intervals; no independent reference

Here we compare pixel-based (MNDWI) and sub-pixel (SAET) shorelines extracted from the same 11 Sentinel-2 scenes (2016 - 2026) and processed with an identical DSAS configuration. We examine whether the signed offset between the two datasets is stable in time and space and how it propagates into end-point and regression rates. We then set that effect against two others that apply whichever method is used: a tidal correction based on the Finite Element Solution 2022 (FES2022) tide model, and the choice of dates from which rates are computed.

2 Study area and data

2.1 Study area

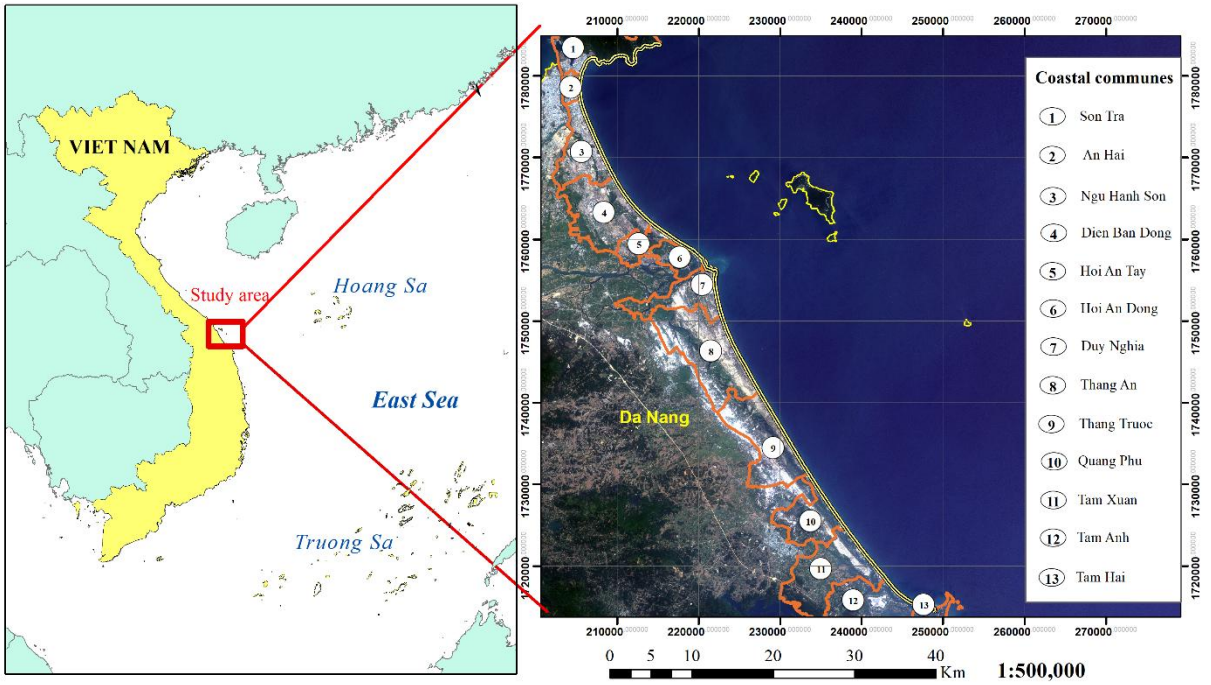


Fig. 1 Study area

The study area comprises about 100 km of open coast of Da Nang City, as delimited after the 2025 administrative reorganisation, from the Son Tra Peninsula (16.12°N) to Tam Hai (15.50°N) (**Fig. 1**). Sandy beaches make up most of the coastline and are interrupted by the rocky Son Tra headland and by the Cua Dai inlet of the Thu Bon River. The tide is mixed, predominantly semi-diurnal near Son Tra and irregular diurnal further south, with a range of 0.5 - 1.2 m that seldom exceeds 2 m (Ngo et al. 2020). Under this microtidal regime, waves,

which are most energetic during the north-east monsoon, exert the dominant control on beach morphology (Ngo et al. 2020). Chronic erosion has affected the Cua Dai area and the Hoi An beaches since the early 2000s (Dinh et al. 2021; Ngo et al. 2020).

2.2 Satellite imagery

We used 11 Level-1C Sentinel-2 scenes from relative orbit R075 (tile T49PBT), one per year from 2016 to 2026, obtained from the Copernicus Data Space Ecosystem (**Table 2**). Because Sentinel-2 is in a sun-synchronous orbit, all scenes were acquired within a narrow window, between about 10:05 and 10:23 local time (UTC+7). Candidate scenes were screened in true-colour composites, because the tile-level cloud statistics and cloud masks were not a reliable guide near the shore; three scenes with cloud or haze over the coast (8 April 2017, 12 April 2022 and 2 April 2023) were rejected in favour of cleaner images. Limiting the selection to clear scenes meant that the acquisitions range from February to April rather than falling in a single month, so some seasonal difference in beach state remains between dates. Both extraction methods depend on the first short-wave infrared band (SWIR1, B11), whose native resolution is 20 m; this, rather than the 10 m resolution of the visible bands, sets the effective pixel size for the comparison.

Table 2 Sentinel-2 scenes and modelled tide at acquisition

No.	Sensor	Date	Time (UTC)	Cloud cover (%)	Processing baseline	Tide at overpass (m, MSL)
1	Sentinel-2A	2016-04-13	03:23:22	0.00	05.00	0.22–0.34
2	Sentinel-2A	2017-02-07	03:09:01	5.78	05.00	0.04–0.05
3	Sentinel-2B	2018-03-19	03:05:39	0.01	05.00	0.17–0.18
4	Sentinel-2A	2019-03-19	03:05:41	0.03	05.00	0.16–0.21
5	Sentinel-2B	2020-03-08	03:05:49	6.94	05.00	0.11–0.17
6	Sentinel-2A	2021-02-26	03:07:01	0.00	05.00	0.04–0.11
7	Sentinel-2A	2022-04-22	03:05:51	2.42	05.10	0.34–0.50
8	Sentinel-2B	2023-04-22	03:05:29	8.82	05.10	0.41–0.49
9	Sentinel-2A	2024-04-01	03:05:21	0.00	05.10	0.26–0.37
10	Sentinel-2B	2025-03-02	03:05:39	0.01	05.11	0.09–0.13
11	Sentinel-2B	2026-03-27	03:05:39	0.00	05.12	0.23–0.30

2.3 Tide model

Astronomical tide at the time of each acquisition was predicted from the FES2022 global tide atlas with the pyfes library, using the extrapolated ocean-tide grids (ocean_tide_extrapolated), which provide values up to the coastline (Aviso 2024; Lyard et al. 2021). Nine principal constituents (M2, S2, N2, K2, K1, O1, P1, Q1 and M4) were used, and minor constituents were inferred by admittance. Predictions were made at three nearshore points located 1 - 2 km offshore, representing the northern (My Khe - Son Tra; 16.05°N, 108.275°E), central (Cua Dai - Hoi An; 15.84°N, 108.43°E) and southern (Tam Hai; 15.51°N, 108.64°E) parts of the coast, and tidal levels at individual transects were later interpolated between these points (**Fig. 2**).

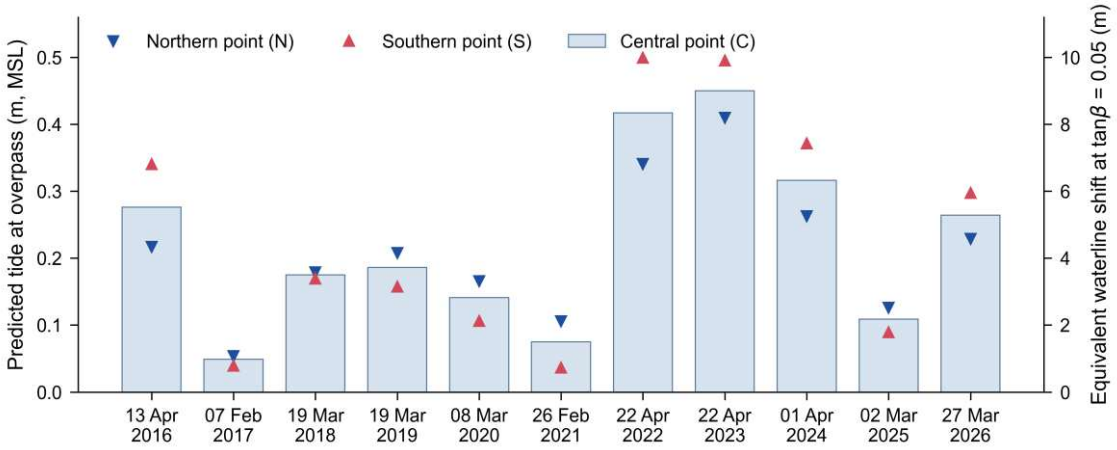


Fig. 2 FES2022 tide at the time of the 11 Sentinel-2 acquisitions at the northern, central and southern points. The right axis gives the waterline shift implied by a beach slope of 0.05

3 Methods

The analysis followed the steps in **Fig. 3**: extraction of shorelines from each scene with the two methods, computation of change statistics in DSAS on a common set of transects, assessment of agreement between the two datasets, and tests of how rates respond to the dates used and to tidal correction.

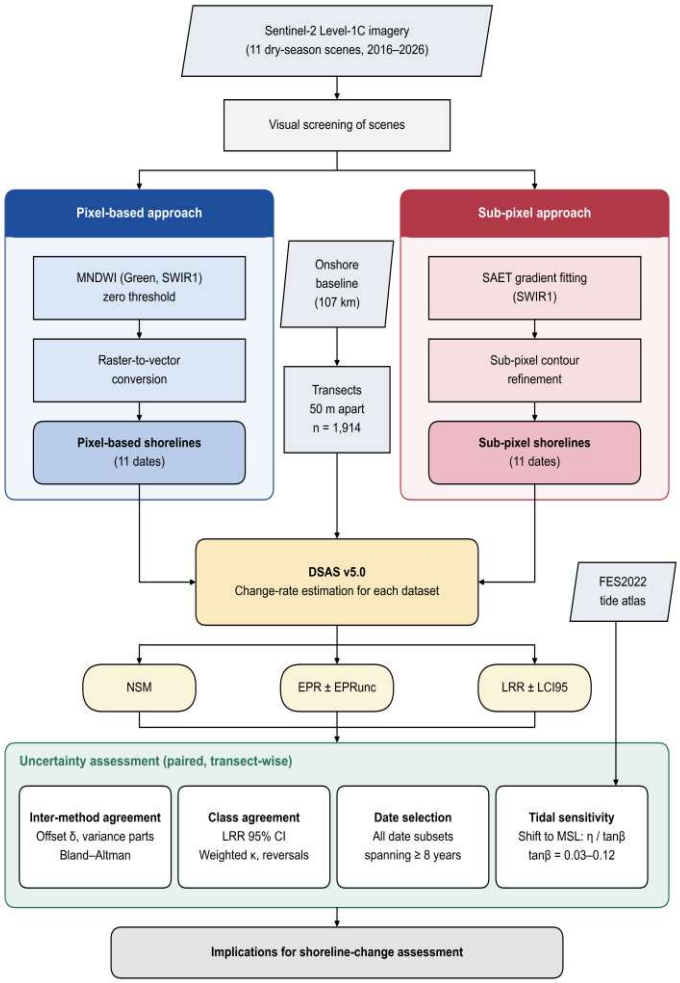


Fig. 3 Workflow of the study. NSM: Net Shoreline Movement; EPR: End Point Rate; EPRunc: EPR uncertainty; LRR: Linear Regression Rate; LCI95: 95% confidence interval of LRR; δ: signed offset; η: tide; tan β: beach slope

3.1 Pixel-based shoreline extraction

MNDWI (Xu 2006) was calculated from top-of-atmosphere reflectance ρ in bands B3 (green) and B11 (SWIR1):

$$\mathrm{MNDWI} = \frac{\rho_{\mathrm{B3}} - \rho_{\mathrm{B11}}}{\rho_{\mathrm{B3}} + \rho_{\mathrm{B11}}} \quad (1)$$

MNDWI was computed on the native 20 m grid of B11, with B3 resampled to 20 m, so the pixel-based shoreline is constrained by a 20 m pixel. Pixels were labelled as water when MNDWI exceeded zero, a fixed threshold applied to all scenes (Dinh et al. 2021; Xu 2006). Because all scenes share the same radiometric offset (**Table 2**), and a common additive offset leaves the numerator of **Eq. 1** unchanged and the denominator positive, the classification at a zero threshold does not depend on whether the offset is removed. The boundary of the binary water mask was vectorised with the ArcGIS Raster to Polygon tool using its default polygon simplification, which replaces the stair-step corners of the raster with straight segments. The polygon of the open sea was retained and only its outer boundary was used, so that lagoons, boats and isolated offshore patches did not contribute to the shoreline.

3.2 Sub-pixel shoreline extraction with SAET

Sub-pixel shorelines were derived with SAET (Palomar-Vázquez et al. 2023), whose core algorithm builds on earlier kernel-based work (Pardo-Pascual et al. 2012; Pardo-Pascual et al. 2018). An approximate shoreline was first obtained at pixel level from an MNDWI mask with a zero threshold, that is, the same index and threshold as in Sect. 3.1, using the morphological dilation option of the tool and no cloud masking. Around that line, SAET analyses the SWIR1 (B11) values within a 3 × 3 pixel kernel (60 × 60 m on the 20 m grid): the values are resampled and fitted with a third-degree polynomial surface, and the shoreline is taken as the contour where the Laplacian of that surface is zero, which corresponds to the maximum slope of the radiometric gradient. Four points were extracted per pixel, equivalent to one point every 5 m, and the same settings were applied to all 11 scenes so that differences between dates could not arise from changes in the processing parameters.

3.3 Trimming of the shorelines

Both datasets were trimmed to the study sector by a single rule that removes line segments without moving any vertex. Boundaries within 1.5 km of the 2016, 2020 and 2025 shorelines, which had first been trimmed by hand, were retained and intersected with the transects described in Sect. 3.4. The seaward crossing of each transect was located, and the line was kept between consecutive crossings unless the path between them exceeded three times their straight-line distance plus 300 m, which marks a detour into a river channel or lagoon. For those three scenes the automated rule reproduced the DSAS intersection distances to within 1 m on 99.0 - 99.6% of transects for the pixel-based lines and on all transects for the sub-pixel lines.

3.4 DSAS configuration and quality control

Shoreline change was computed with DSAS v5.0 in ArcMap 10.4 (Himmelstoss et al. 2018). A 107 km baseline was digitised onshore of all shorelines, and 2,144 transects were cast from it at 50 m intervals, with a length of 8,500 m and a smoothing distance of 2,500 m (**Fig. 4**). Transects were not clipped to the shoreline extent, so that exactly the same transects intersected the pixel-based and the sub-pixel datasets. Where a transect crossed a shoreline more than once, DSAS retained the seaward intersection. A positional uncertainty of 10 m was assigned

to each shoreline, in line with the horizontal accuracy of about 10 m reported for satellite-derived shorelines at microtidal sites (Vos et al. 2023).

Of the 2,144 transects, 115 reached no shoreline on any date, at the two ends of the baseline and where it turns around the north-western corner of the Son Tra Peninsula, and 43 did not intersect all 11 shorelines of both datasets, which left 1,986 transects for further screening. Two inlet sectors were then excluded: the Cua Dai inlet (transects 1122 - 1144) and the inlet at Tam Hai at the southern end of the baseline (transects 1 - 57), which together removed 13 of the remaining transects; three more (1874, 1875 and 2118), whose crossings fell at the very end of a line section, were also dropped. At Cua Dai, the raw SAET line spanned the open water of the inlet with a straight segment of 416 - 1,030 m on every date; at Tam Hai, the lines followed different banks of the channel from one date to the next. Crossings in these sectors therefore do not record the displacement of a single, continuous shoreline and cannot be interpreted as shoreline change. A further 56 transects, mostly in the coves of the Son Tra headland, crossed at least one shoreline more than once; their rates depend on which crossing is retained, and they were also removed. After these exclusions, 1,914 transects (89.3% of those cast) remained, and all subsequent analyses are based on this common set.

Net Shoreline Movement (NSM), End Point Rate (EPR) with its uncertainty (EPRunc), and Linear Regression Rate (LRR) were taken from DSAS. Because all shorelines carry the same uncertainty, the weighted regression rate is identical to LRR and is not reported separately. Rates were recomputed from the DSAS intersection tables as a check, and differed from the DSAS output by no more than 0.008 m yr^{-1}, the rounding of the DSAS tables. DSAS was run with a 90% confidence level; the 95% confidence intervals of LRR (LCI95) reported here were derived from the same regressions using Student's *t* with 9 degrees of freedom. Transects were assigned to the nearest ward or commune using the post-2025 administrative boundaries.

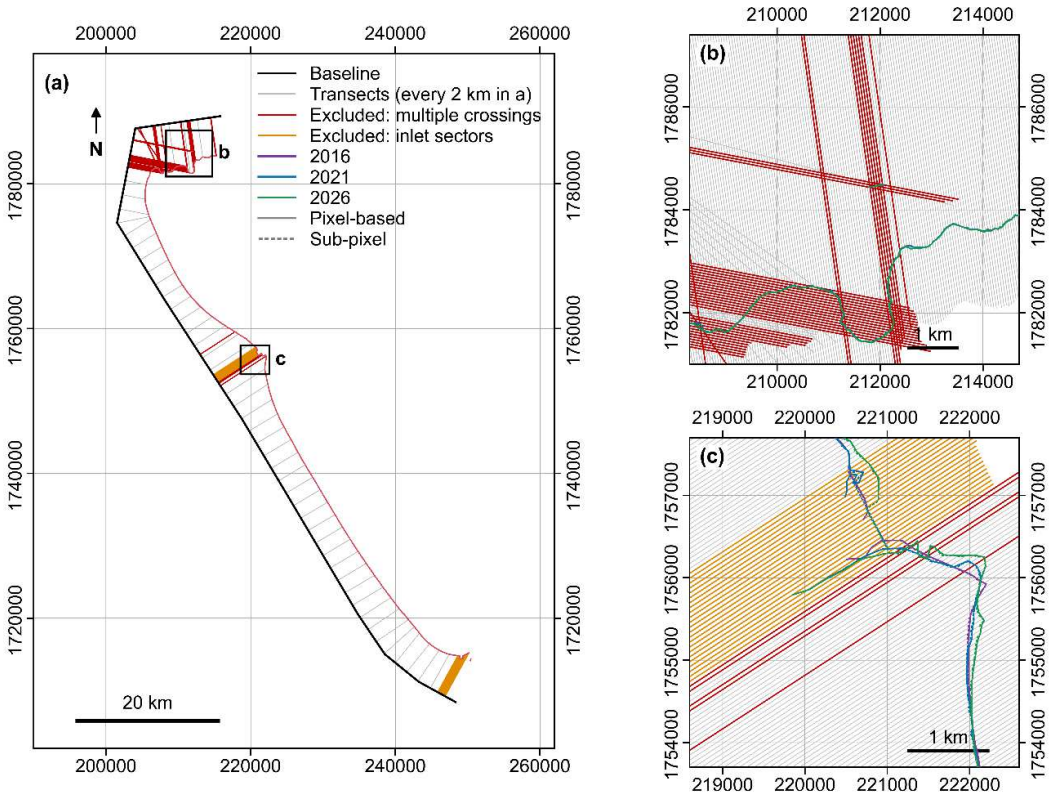


Fig. 4 DSAS configuration. (a) Baseline and transects along the study coast; transects were cast every 50 m (n = 2,144), and only every 40th transect is drawn for legibility. Transects excluded because they crossed a shoreline

more than once (red) or lay in inlet sectors (orange) are highlighted; boxes mark panels b and c. (b) Son Tra headland, where shoreline curvature produced multiple crossings. (c) Cua Dai inlet, showing pixel-based (solid) and sub-pixel (dashed) shorelines for 2016, 2021 and 2026

3.5 Agreement between shoreline datasets

For transect i and date t, the signed offset between the two methods was calculated from the DSAS intersection distances D, measured from the baseline and increasing seaward:

$$\delta_{i,t} = D_{i,t}^{\mathrm{sub}} - D_{i,t}^{\mathrm{pix}} \quad (2)$$

Negative values of δ indicate that the pixel-based shoreline lies seaward of the sub-pixel shoreline. Since EPR is the displacement between the oldest and most recent shorelines divided by the elapsed time Δt (9.95 years), the difference in EPR between the two methods reduces to a function of the offsets at the two end dates:

$$\Delta\mathrm{EPR}_i = \mathrm{EPR}_i^{\mathrm{sub}} - \mathrm{EPR}_i^{\mathrm{pix}} = \frac{\delta_{i,2026} - \delta_{i,2016}}{\Delta t} \quad (3)$$

Likewise, the difference in LRR (ΔLRR) equals the slope of δ regressed on time at that transect, so that all dates contribute. These are identities and explain nothing by themselves; what matters empirically is how large and how persistent δ is. A coast-wide constant offset would cancel completely in the rate, whereas an offset that varies independently between dates at each transect would add scatter even if its mean did not change.

The persistence of δ was assessed in two complementary ways. First, we computed the correlation of δ between all pairs of dates across transects, both for individual transects and for means over 1 km blocks. Second, we partitioned the variance of δ with a two-way analysis of variance without replication into components for transect, date and residual, and derived the corresponding intraclass correlation (Shrout and Fleiss 1979). Agreement in shoreline position and in rates was summarised by Bland - Altman analysis, that is, by the mean difference (bias) and the 95% limits of agreement, bias ± 1.96 standard deviations (SD) (Bland and Altman 1986).

To assess consequences for erosion mapping, each transect was assigned to one of three classes according to whether the LCI95 of its LRR excluded zero: erosion (LRR < 0), accretion (LRR > 0) or otherwise stable. For comparison, classes were also derived from the sign of LRR, from fixed LRR thresholds of 0.5 and 1.0 m yr^{-1}, and from EPR with EPRunc as the threshold. Class agreement between methods was expressed as the percentage of matching transects and as linearly weighted Cohen's kappa (Cohen 1968), interpreted following Landis and Koch (1977). We refer to a transect classified as eroding by one method and accreting by the other as a reversal.

Because neighbouring transects 50 m apart are spatially autocorrelated, tests applied to all 1,914 transects would overstate statistical significance. The Wilcoxon signed-rank test was therefore repeated on a subsample of every fourth transect (200 m spacing; n = 479), and 95% confidence intervals (CI) for coast-mean rates, their differences, kappa and the proportion of sign disagreement were estimated with a moving-block bootstrap (blocks of 20 transects, i.e. 1 km; 2,000 replicates) (Künsch 1989).

3.6 Sensitivity to the dates used

To measure how far rates depend on the choice of images, the regression rate was recalculated at every transect for each subset of 2 to 10 of the 11 dates whose first and last dates were at least 8 years apart (1,279 subsets). For subsets of two dates the regression rate is identical to the EPR, so these subsets also describe the sensitivity of end-point rates to the choice of dates. For each subset we recorded the coast-mean rate of each method, the difference between methods and the departure from the rate obtained with all 11 dates. The 11-date

rate serves here as a common point of comparison and is not assumed to be the true rate. Coast-mean LRR was also recomputed with each date left out in turn.

3.7 Sensitivity to tidal correction

Tidal levels at each transect were interpolated linearly with latitude between the three FES2022 prediction points, and each shoreline was shifted along its transect to mean sea level (MSL):

$$D_{i,t}^{\mathrm{MSL}} = D_{i,t} + \frac{\eta_{i,t}}{\tan\beta} \quad (4)$$

where η is the predicted tide at acquisition relative to MSL and tan β is the intertidal beach slope. A positive η implies a waterline displaced landward of its MSL position, so the correction moves the shoreline seaward. In the absence of beach-profile surveys for the study area, the correction was applied for tan β = 0.03, 0.05, 0.08 and 0.12, which spans the range commonly observed on dissipative to intermediate sandy beaches (Vos et al. 2020). Rates and classes were recalculated for each slope and for both methods.

All post-processing of the DSAS outputs was carried out in Python 3.9 using pandas, SciPy, scikit-learn and Shapely.

4 Results

4.1 Offset between pixel-based and sub-pixel shorelines

On every date the pixel-based shoreline lay seaward of the sub-pixel shoreline on most transects, between 87.1% and 96.4% depending on the date (**Table 3**; **Fig. 5** and **Fig. 6**a). The mean offset ranged from -4.83 m in 2017 to -7.58 m in 2016, roughly one quarter to two fifths of a 20 m SWIR1 pixel, and averaged -6.27 m over all dates (block-bootstrap 95% CI -6.50 to -6.04 m). The spread of the offsets was similar from date to date, with standard deviations of 4.1 - 4.6 m, so no single scene was markedly less consistent than the others. Along most of the coast the running median of the transect means stayed close to the overall mean, whereas scatter increased towards the Cua Dai sector and on the Son Tra coast (**Fig. 7**).

Table 3 Signed offset δ (sub-pixel − pixel-based) along transects (n = 1,914)

Year	Bias (m)	Median (m)	SD (m)	Limits of agreement (m)	Mean $\lvert\delta\rvert$ (m)	RMS (m)	Pixel-based seaward (%)
2016	-7.58	-7.93	4.44	-16.28 to 1.12	7.82	8.79	96.3
2017	-4.83	-4.68	4.62	-13.88 to 4.23	5.45	6.68	87.1
2018	-5.43	-5.64	4.51	-14.26 to 3.41	6.04	7.05	90.5
2019	-6.49	-6.43	4.15	-14.63 to 1.65	6.72	7.71	95.6
2020	-5.62	-5.70	4.33	-14.10 to 2.87	6.08	7.09	92.6
2021	-5.98	-6.01	4.58	-14.96 to 2.99	6.40	7.53	93.1
2022	-5.84	-5.61	4.48	-14.63 to 2.95	6.14	7.36	93.3
2023	-7.15	-7.18	4.12	-15.21 to 0.92	7.33	8.25	96.4
2024	-7.42	-7.52	4.25	-15.76 to 0.91	7.62	8.55	96.4
2025	-5.86	-5.78	4.37	-14.44 to 2.71	6.23	7.31	91.4
2026	-6.77	-6.73	4.09	-14.79 to 1.26	7.02	7.91	96.3

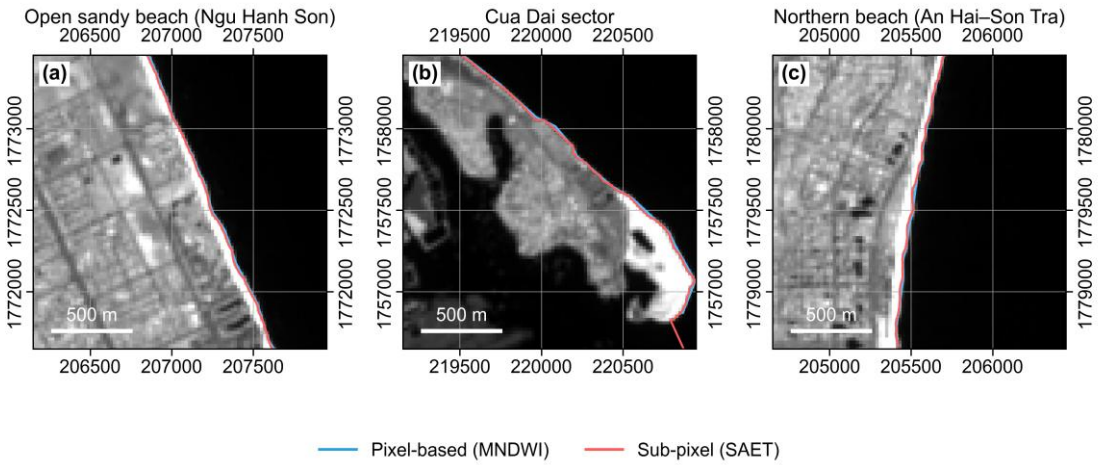


Fig. 5 Pixel-based and sub-pixel shorelines of 2025 at three sites on the Sentinel-2 SWIR1 (B11) image of the same date, shown at its native 20 m grid. Coordinates: WGS 84 / UTM zone 49N

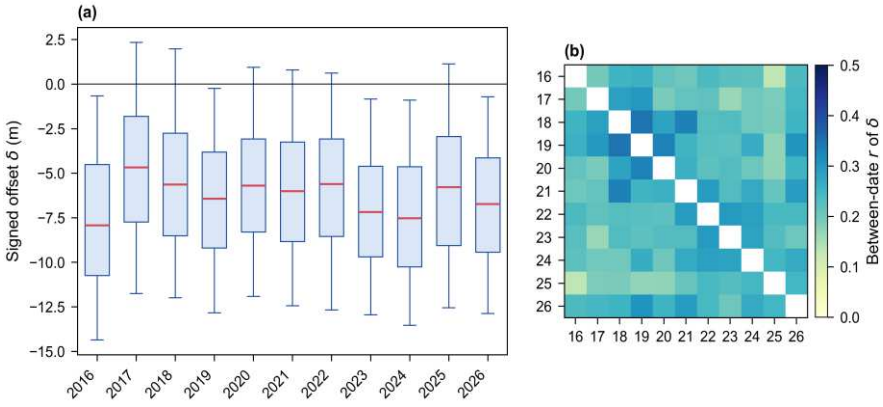


Fig. 6 (a) Signed offset δ (sub-pixel − pixel-based) on each date; boxes: interquartile range, red line: median, whiskers: 5th and 95th percentiles. (b) Correlation of δ across transects between pairs of dates (years 2016 - 2026)

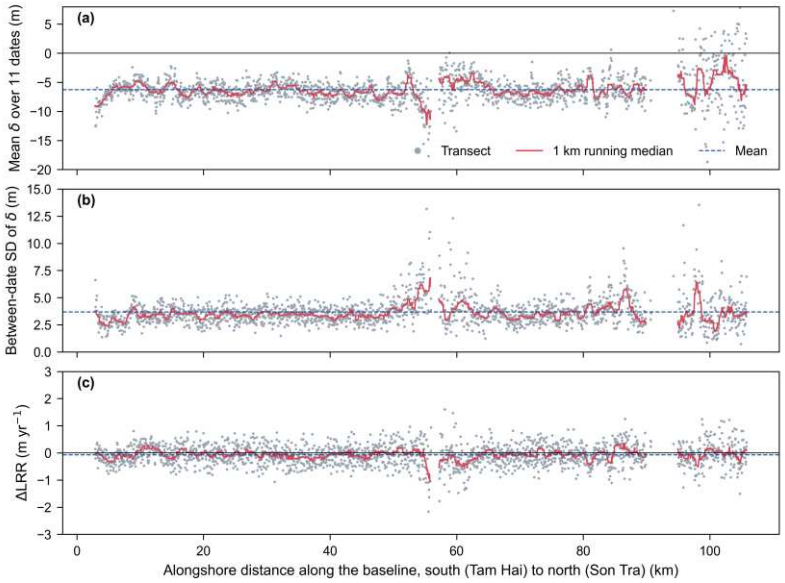


Fig. 7 Alongshore distribution of (a) the mean of δ over the 11 dates, (b) its between-date SD and (c) ΔLRR (sub-pixel − pixel-based). Distance is measured along the baseline; gaps correspond to excluded transects. A few transects lie outside the plotted range in a and c

The mean offset was thus fairly stable, but its value at a given transect was not. Between pairs of dates, offsets at individual transects correlated with r = 0.13 - 0.35 (mean 0.24; **Fig. 6**b). Averaging over 1 km blocks raised the correlation to 0.22 - 0.71 (mean 0.49), so part of the alongshore pattern does persist at that scale. In the variance partition, differences between transects accounted for 23.0% of the variance of δ, differences between dates for 3.9% and the residual, which is the transect-by-date variation, for 73.2%; the intraclass correlation was 0.24.

Across the 11 dates, the median offset grew in magnitude with predicted tide (r = -0.58, p = 0.063) and with later acquisition in the year (r = -0.68, p = 0.022), but neither rank correlation was significant (p = 0.096 and 0.127), and predicted tide and acquisition date were themselves closely related in this set of images (r = 0.95), so their effects cannot be separated. The two sensors did not differ (mean of date medians -6.36 m for Sentinel-2A, -6.21 m for Sentinel-2B; Mann - Whitney p = 0.93). These tests are exploratory, given 11 dates and no correction for multiple comparisons.

4.2 Shoreline change derived from each method

The two datasets reproduced the same alongshore pattern of change (**Fig. 8**). LRR was within ±1 m yr^{-1} on 65.2% (pixel-based) and 66.0% (sub-pixel) of transects, and most transects were stable within their 95% confidence interval: significant erosion affected 3.6% and 4.1%, and significant accretion 9.5% and 10.0%, respectively (**Table 4**). The strongest regression retreat occurred in Hoi An Tay (-4.50 and -4.80 m yr^{-1} at transects 1236 and 1235) and the strongest advance on the sand body south of the Cua Dai inlet, in Duy Nghia (+46.3 and +46.3 m yr^{-1}).

LRR and EPR, however, described the coast differently: mean LRR was positive for both methods (+0.64 and +0.57 m yr^{-1}; block-bootstrap 95% CI 0.29 - 1.17 and 0.22 - 1.04), whereas mean EPR was close to zero (-0.13 and -0.05 m yr^{-1}; CI -0.46 to 0.29 and -0.38 to 0.32), and 62.3% and 56.1% of transects had a negative EPR, against 32.3% and 34.6% for LRR. The reason for this contrast is apparent in **Fig. 9**: mean shoreline position fluctuated from date to date over a range of 14.6 m (sub-pixel) and 17.2 m (pixel-based), and the first date, in 2016, lay well seaward of the following years, whereas the regression uses all dates. These fluctuations were almost identical for the two methods (r = 0.996) and were not significantly related to tide (r = 0.40, p = 0.23) or to acquisition date within the year (r = 0.47, p = 0.15).

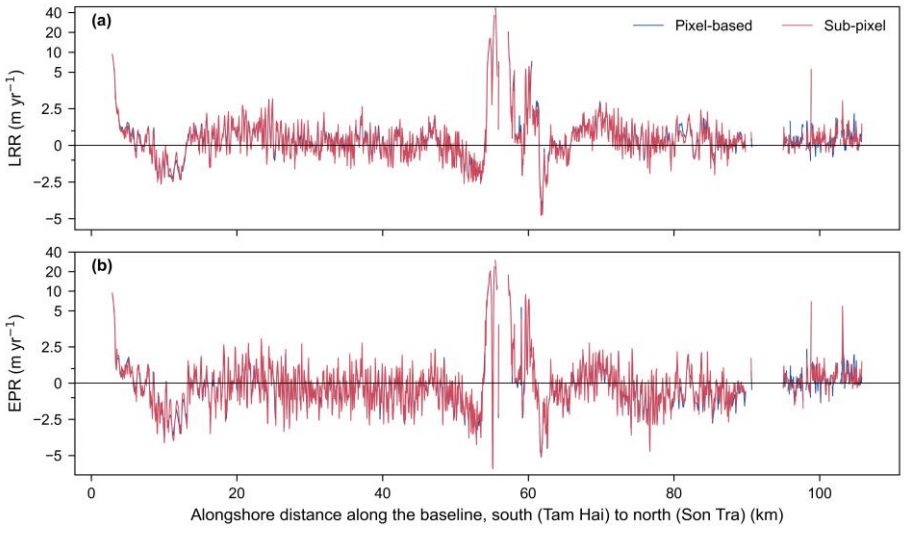


Fig. 8 Alongshore (a) LRR and (b) EPR from both methods, from south (Tam Hai) to north (Son Tra). Rate axes are linear between -5 and 5 m yr^{-1} and logarithmic beyond

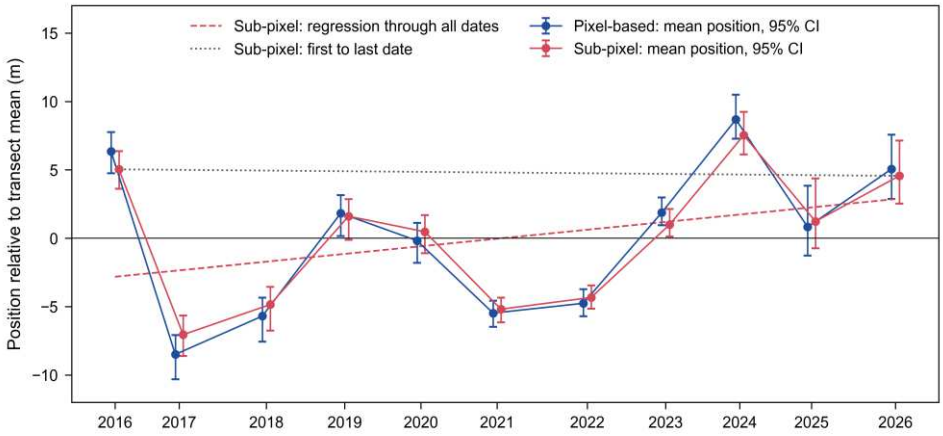


Fig. 9 Mean shoreline position on each date relative to the 11-date mean at each transect (positive seaward), with block-bootstrap 95% confidence intervals, compared with the regression through all dates and the line joining the first and last dates

Table 4 DSAS statistics for the 1,914 analysed transects

Metric	Pixel-based	Sub-pixel
Mean NSM (m)	-1.30	-0.48
Median NSM (m)	-3.36	-1.56
Mean EPR (m yr^{-1})	-0.13	-0.05
Median EPR (m yr^{-1})	-0.34	-0.16
EPR range (m yr^{-1})	-6.90 to 29.68	-8.07 to 29.50
Transects with EPR < 0 (%)	62.3	56.1
Significant erosion, EPR (%)	18.5	18.7
Significant accretion, EPR (%)	7.8	9.7
Mean LRR (m yr^{-1})	0.64	0.57
Median LRR (m yr^{-1})	0.40	0.31
LRR range (m yr^{-1})	-4.50 to 46.29	-4.80 to 46.31
Transects with LRR < 0 (%)	32.3	34.6
Significant erosion, LRR (%)	3.6	4.1
Significant accretion, LRR (%)	9.5	10.0

Rates and the frequency of significant change also differed considerably between wards and communes (**Table 5**). Significant erosion was most frequent at Duy Nghia, Hoi An Tay and Tam Xuan, while accretion was most frequent at Hoi An Dong, Tam Hai and Dien Ban Dong. At Duy Nghia, transects with significant erosion and significant accretion occurred side by side, the latter on the sand body bordering the inlet.

Table 5 Linear Regression Rate (m yr^{-1}) and classes by ward and commune (classes from LCI95)

Ward / commune (N to S)	n	Pixel-based LRR, median (P5 to P95)	Sub-pixel LRR, median (P5 to P95)	Erosion (%), P / S	Accretion (%), P / S	Same class (%)	Mean ΔLRR
Son Tra	243	0.31 (-0.32 to 1.43)	0.28 (-0.30 to 1.39)	0.4 / 0.8	12.3 / 17.3	83.1	-0.02
An Hai	51	-0.01 (-1.09 to 0.81)	0.11 (-1.10 to 1.19)	0.0 / 2.0	0.0 / 0.0	98.0	0.12
Ngu Hanh Son	268	0.48 (-0.84 to 1.67)	0.42 (-0.87 to 1.77)	0.0 / 0.0	1.9 / 2.2	98.9	-0.08
Dien Ban Dong	143	1.17 (-0.70 to 2.33)	1.01 (-0.71 to 2.30)	0.0 / 2.1	33.6 / 27.3	81.8	-0.08
Hoi An Tay	80	-0.28 (-3.80 to 2.78)	-0.47 (-4.23 to 2.15)	13.8 / 20.0	0.0 / 0.0	91.2	-0.24
Hoi An Dong	70	1.95 (-0.77 to 7.68)	1.73 (-0.79 to 7.49)	1.4 / 7.1	50.0 / 50.0	80.0	-0.22
Duy Nghia	107	-0.87 (-2.21 to 23.69)	-0.87 (-2.43 to 23.21)	21.5 / 23.4	20.6 / 21.5	86.0	-0.09
Thang An	205	0.18 (-1.02 to 1.28)	0.15 (-1.41 to 1.30)	2.0 / 1.5	1.0 / 3.4	94.1	-0.06
Thang Truong	235	0.31 (-0.67 to 1.38)	0.13 (-0.87 to 1.49)	0.0 / 1.3	3.0 / 3.0	96.2	-0.13

Ward / commune (N to S)	n	Pixel-based LRR, median (P5 to P95)	Sub-pixel LRR, median (P5 to P95)	Erosion (%), P / S	Accretion (%), P / S	Same class (%)	Mean ΔLRR
Quang Phu	158	0.83 (-0.85 to 2.34)	0.73 (-0.86 to 2.47)	0.0 / 0.0	6.3 / 7.0	96.8	-0.02
Tam Xuan	200	0.45 (-2.12 to 1.65)	0.35 (-2.06 to 1.85)	11.5 / 8.0	1.5 / 3.0	91.0	0.01
Tam Anh	117	-0.02 (-1.94 to 1.35)	-0.06 (-2.17 to 1.13)	4.3 / 3.4	0.0 / 0.0	97.4	-0.11
Tam Hai	37	1.86 (0.87 to 8.06)	1.59 (0.69 to 7.98)	0.0 / 0.0	51.4 / 40.5	89.2	-0.08

4.3 Propagation of the offset into rates

The mean difference between methods was small and in opposite directions for the two rate metrics: ΔLRR = -0.07 m yr^{-1} (block-bootstrap 95% CI -0.10 to -0.04) and ΔEPR = +0.08 m yr^{-1} (CI 0.06 to 0.11). Correlations between methods were high (r = 0.990 for LRR, 0.977 for EPR; **Fig. 10**). At the scale of individual transects the limits of agreement were -0.84 to +0.70 m yr^{-1} for LRR (mean absolute error, MAE, 0.31 m yr^{-1}; root mean square error, RMSE, 0.40 m yr^{-1}) and -0.96 to +1.12 m yr^{-1} for EPR (MAE 0.43 m yr^{-1}; RMSE 0.54 m yr^{-1}). The corresponding mean difference in NSM was +0.82 m (MAE 4.27 m). Paired differences in LRR remained significant whether all transects were used (Wilcoxon $p = 1.3 \times 10^{-15}$, n = 1,914) or only those spaced 200 m apart ($p = 3.7 \times 10^{-6}$, n = 479), although their size is small.

The size of this scatter is consistent with the weak persistence of the offsets reported in Sect. 4.1: if offsets were independent between dates, their mean between-transect SD of 4.4 m would yield an SD of ΔLRR of 0.41 m yr^{-1}; the observed value was 0.39 m yr^{-1}. For ΔEPR, the corresponding expected and observed values were 0.61 and 0.53 m yr^{-1}. Using all 11 dates narrowed the transect-level difference: on the same transects, the three scenes of 2016, 2020 and 2025 gave an SD of the rate difference of 0.65 m yr^{-1}.

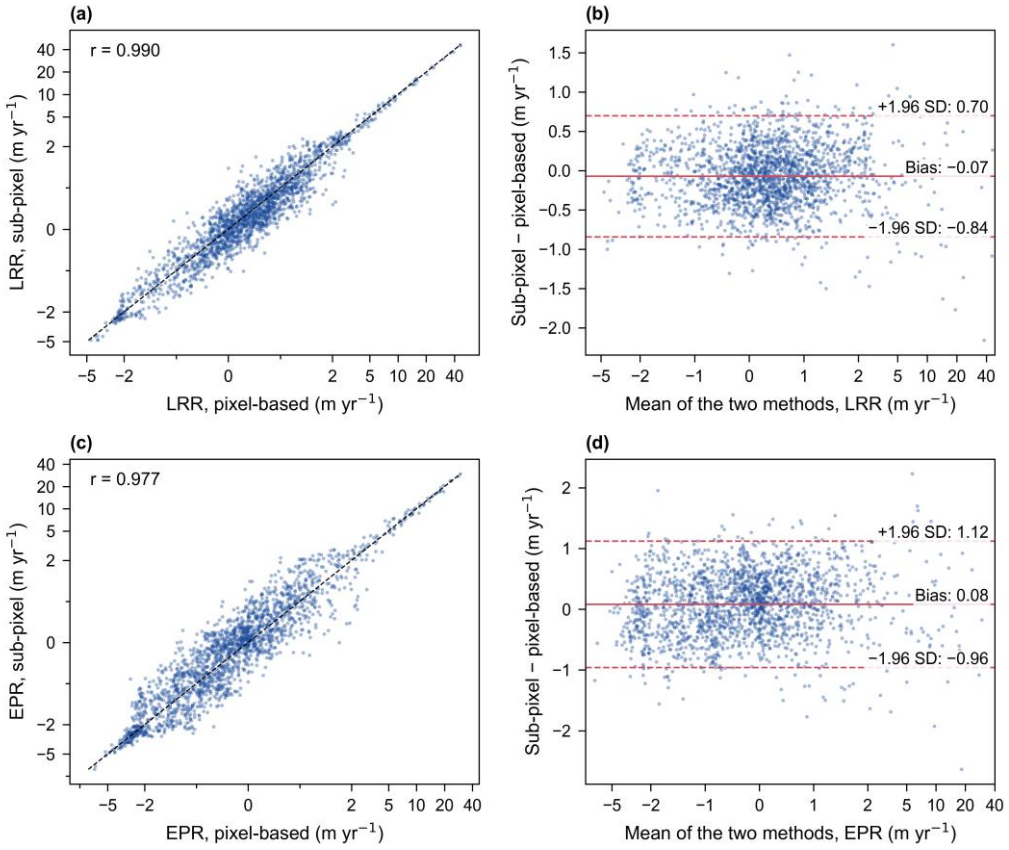


Fig. 10 Comparison of (a) LRR and (c) EPR from pixel-based and sub-pixel shorelines (dashed line: 1:1), and Bland–Altman plots of (b) LRR and (d) EPR (solid line: bias; dashed lines: limits of agreement). Rate axes are linear between −2 and 2 m yr^{-1} and logarithmic beyond

4.4 Agreement in erosion – stable - accretion classes

With classes based on LCI95, 91.7% of transects fell in the same class with both methods (weighted $\kappa = 0.67$, block-bootstrap 95% CI 0.59 - 0.74; **Table 6**; **Fig. 11**), which spans moderate to substantial agreement on the scale of Landis and Koch (1977). The value of κ is held down by the rarity of the erosion and accretion classes: of 68 transects classed as eroding by the pixel-based data, 46 were also eroding in the sub-pixel data, as were 134 of 181 accreting transects. None of the transects showed a reversal, that is, erosion with one method and accretion with the other. This result should not be over-interpreted, however, because the stable class is wide (median LCI95 about 1.8 m yr^{-1}). When classes were defined by the sign of LRR alone, 12.0% of transects reversed (bootstrap CI 9.9 - 14.2%), and these were mainly transects with rates close to zero (median |LRR| 0.21 m yr^{-1}, against 0.79 m yr^{-1} for the rest).

Disagreement between the two methods was not evenly distributed along the coast (**Table 5**). Agreement was lowest at Hoi An Dong (80.0%), Dien Ban Dong (81.8%) and Son Tra (83.1%) and exceeded 96% at An Hai, Ngu Hanh Son, Thang Truong, Quang Phu and Tam Anh. Among units with at least 50 transects, the largest difference in the share of eroding transects was 6.2 percentage points, at Hoi An Tay.

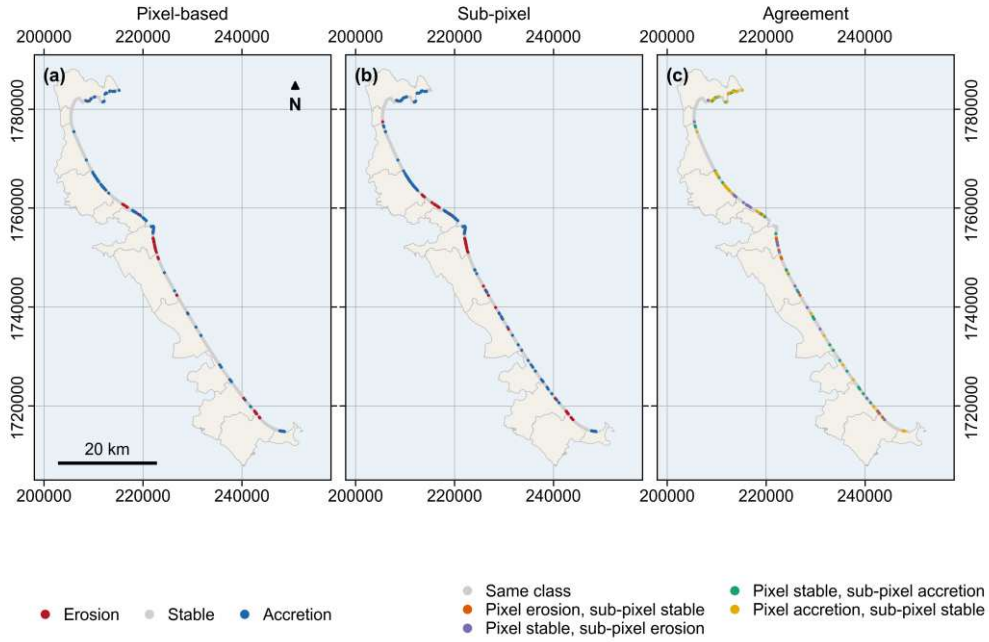


Fig. 11 Erosion, stable and accretion classes based on the 95% confidence interval of LRR from (a) pixel-based and (b) sub-pixel shorelines, and (c) class agreement between the methods. Coordinates: WGS 84 / UTM zone 49N

Table 6 Class agreement between methods under different stability criteria

Stability criterion	Agreement (%)	Weighted κ	Reversals (%)	Pixel-based erosion / stable / accretion (%)	Sub-pixel erosion / stable / accretion (%)
LRR, LCI95 excludes zero	91.7	0.67	0.0	3.6 / 87.0 / 9.5	4.1 / 85.9 / 10.0
LRR, sign only	88.0	0.73	12.0	32.3 / 0.0 / 67.7	34.6 / 0.0 / 65.4
LRR, ± 0.5 m yr^{-1}	79.2	0.74	0.1	16.9 / 37.7 / 45.4	19.7 / 38.7 / 41.6
LRR, ± 1.0 m yr^{-1}	87.4	0.77	0.0	9.8 / 65.2 / 25.0	10.8 / 66.0 / 23.2
EPR, ± EPRunc (≈ 1.42 m yr^{-1})	86.9	0.72	0.0	18.5 / 73.6 / 7.8	18.7 / 71.6 / 9.7

4.5 Sensitivity to the dates used

The coast-mean rate depended strongly on which dates were used (**Table 7**; **Fig. 12**). Among three-date subsets spanning at least 8 years, the mean sub-pixel rate ranged from -0.60 to +1.48 m yr^{-1}. For the subset of 2016, 2020 and 2025 specifically, it was -0.40 m yr^{-1} (pixel-based -0.59 m yr^{-1}), with 64.6% of transects retreating, which would suggest net erosion. Over the same transects, all 11 dates gave +0.57 m yr^{-1} (pixel-based +0.64 m yr^{-1}), with 34.6% retreating. End-point rates behaved similarly: with a start date in 2016 - 2018 and an end date in 2024 - 2026, mean sub-pixel EPR ranged from -0.43 to +2.05 m yr^{-1} and the share of transects with a negative EPR from 15.4% to 64.6%.

By comparison, the mean difference between methods within a subset was small: 0.14 m yr^{-1} on average for three dates and never above 0.25 m yr^{-1}. At transect level, three-date rates departed from the 11-date rate by 0.99 m yr^{-1} on average and had the opposite sign on 25.0% of transects, whereas the method difference on the same subsets had an SD of 0.60 m yr^{-1}. The range narrowed as dates were added, yet with nine dates the coast-mean rate still spanned 0.10 to +1.25 m yr^{-1}. Removing any single date from the full set left mean LRR positive (0.34–1.08 m yr^{-1} for the sub-pixel data); the extremes occurred when 2017 and 2016 were removed, respectively.

Table 7 Effect of the dates used on regression rates, for subsets whose first and last dates are at least 8 years apart

Dates in subset	Subsets	Coast-mean rate, range (m yr^{-1})	Mean |method difference| (m yr^{-1})	SD of method difference (m yr^{-1})	MAE vs 11 dates (m yr^{-1})	Sign differs from 11 dates (%)
2 (EPR)	5	−0.43 to 1.27	0.16	0.63	1.07	25.9
3	39	−0.60 to 1.48	0.14	0.60	0.99	25.0
5	266	−0.64 to 1.58	0.12	0.54	0.80	21.5
7	280	−0.52 to 1.47	0.09	0.48	0.59	17.1
9	54	0.10 to 1.25	0.08	0.43	0.37	11.0
10	11	0.34 to 1.08	0.07	0.41	0.22	6.7
11	1	0.57	0.07	0.39	–	–

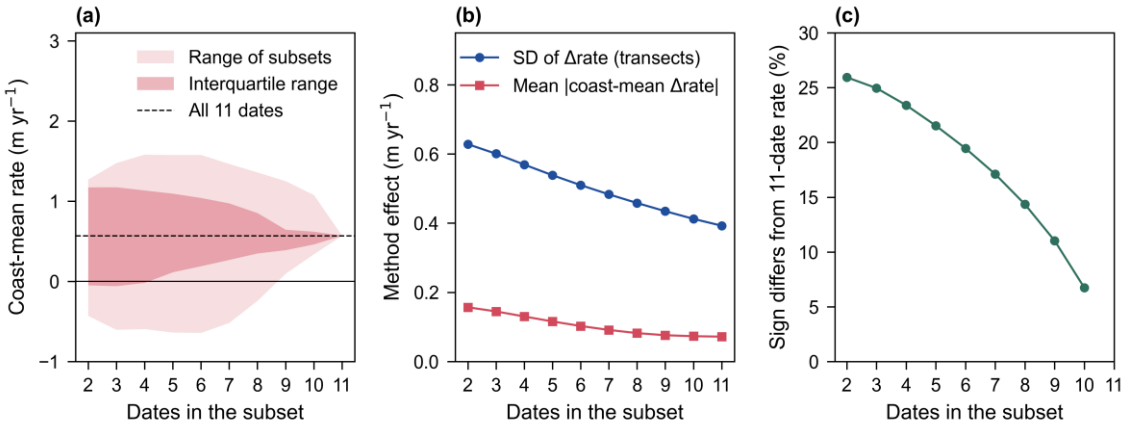


Fig. 12 Effect of the dates used, for all subsets whose first and last dates are at least 8 years apart: (a) coast-mean sub-pixel rate; (b) method effect on the rate; (c) share of transects whose sub-pixel rate has a sign unlike the 11-date rate

4.6 Sensitivity to tide correction

Predicted tide at overpass ranged from 0.04 to 0.50 m above MSL across scenes and points (**Fig. 2**). The tide tended to be higher in the later scenes, particularly in 2022 - 2024, so removing its effect increased mean LRR: by 0.11 m yr^{-1} for tan β = 0.12 and by 0.45 m yr^{-1} for tan β = 0.03 (**Fig. 13**). Significant erosion declined from 3.6% to 0.2 - 2.6% (pixel-based) and from 4.1% to 0.8 - 3.1% (sub-pixel), and 2.9 - 6.9% of sub-pixel transects changed

class. Because the correction is the same for both datasets, ΔLRR (-0.07 m yr^{-1}) did not change, and kappa stayed between 0.64 and 0.69.

For end-point rates, the effect of the correction depended on the difference in tidal level between the two end dates. Between 2016 and 2026, whose tidal levels were similar, mean EPR changed by -0.011 to -0.045 m yr^{-1}. Between 2016 and 2025, the tide was lower in the later scene by 0.09–0.25 m across the three points, and the same correction changed mean EPR by -0.16 to -0.63 m yr^{-1}.

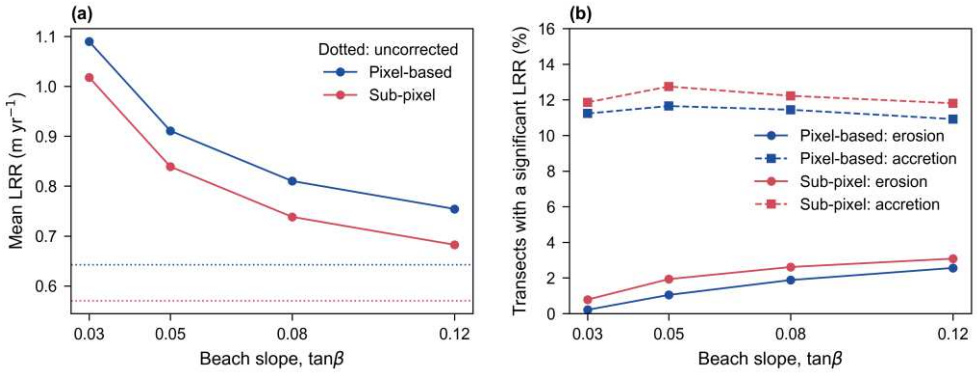


Fig. 13 (a) Mean LRR and (b) share of transects with a significant LRR after tide correction, as a function of beach slope

5 Discussion

5.1 Transfer of the inter-method offset to change rates

The seaward position of the pixel-based line is consistent with the way the two approaches treat the land–water transition. Both start from an MNDWI mask with a zero threshold, so the offset of about 5–8 m must arise mainly from what happens after that step: the pixel-based workflow assigns each boundary pixel entirely to one class and vectorises its edge, whereas SAET moves the line to the steepest SWIR1 gradient within the transition zone (Palomar-Vázquez et al. 2023). The polygon simplification of the pixel-based line, which replaces stair-steps with straight segments, may also contribute. The developers of SAET note that the kernel can displace the line landward on narrow beaches next to vegetation, which may be relevant on parts of this coast but was not tested here. The offset by itself cannot show which line lies closer to the true waterline.

The common argument that a systematic offset cancels in a change rate is correct only for the part that persists. In our data this holds at coast scale, where the mean offset varied by less than 3 m between dates and the rate difference was below 0.1 m yr^{-1}. At the scale of individual transects, however, it does not: most of the variance in the offset was transect-by-date variation, and offsets correlated only weakly between dates, so the observed scatter of ΔLRR and ΔEPR was close to what independent offsets would produce. Some of this variation probably reflects how a 20 m grid intersects the shoreline at different positions in different images, which would explain why correlation between dates improved when offsets were averaged over 1 km, although this mechanism was not tested directly. Method comparisons based on a single date, or on mean offsets alone, would miss this component.

The transect-level effect also depends on the number of dates, because regression averages the date-specific offsets; the SD of the rate difference fell from 0.65 m yr^{-1} with three dates to 0.39 m yr^{-1} with 11. In a multi-date analysis, then, the choice between these two methods matters less than it does for a two-date or three-date comparison.

5.2 Date selection compared with extraction method

The largest effect in our analysis did not come from the extraction method. Three-date subsets of the same data produced coast-mean rates ranging over about 2.1 m yr^{-1}, more than an order of magnitude above the mean difference between the methods, and the subset of 2016, 2020 and 2025 pointed to net retreat where the full record did not. This does not mean that one subset is wrong: each measures real positions on its dates. Rather, year-to-year variation in shoreline position, about 15 m in the coast-wide mean, is large compared with the net change over a decade, and a rate from few dates inherits that variation. Satellite records can resolve variability of this kind (Vos, Harley, et al. 2019). On a much larger and more energetic coast in south-west France, interannual variability in satellite-derived shorelines followed winter wave conditions, and alongshore averaging helped to expose its drivers (Castelle et al. 2022). Our data contain no wave information, so we can say only that tide and acquisition date within the year did not significantly account for the fluctuations we observed.

These results have a direct consequence for erosion assessment. Because the direction of the coast-wide signal changed with both the rate metric and the dates used, a statement that a coast is eroding or accreting based on few dates should be read with caution. The positive mean LRR found here should itself not be taken as evidence of a coast-wide advance: 86% of sub-pixel transects were statistically stable, its value depends on the inclusion of particular years (0.34 - 1.08 m yr^{-1} when single dates were removed), and seasonal differences between images were not controlled. Regression through many dates is less exposed to single images than EPR, which rests on two, and the literature has long debated the relative merits of such methods (Genz et al. 2007). We recommend that assessments report rate sensitivity to date selection, for example by leaving out each date in turn, alongside the rates themselves. Where few dates are available, an image-selection test of this kind costs little and may be more informative than a comparison of extraction methods.

5.3 Implications for classification and coastal management

Coast-wide agreement in classes was high, and the methods did not produce any reversal under an uncertainty-based criterion. That outcome owes much to the wide stable class, so it is not in itself evidence of close agreement. Using sign alone, about 12% of transects reversed, mostly where rates were near zero. At local level, some units showed larger differences than the coast-wide statistics suggest, and agreement fell to 80 - 83% at Hoi An Dong, Dien Ban Dong and Son Tra, where significant accretion was relatively common. A setback or erosion map (Ngo et al. 2020) built with one method could therefore change its message locally even though the coast-wide figures look reassuring. We recommend an uncertainty-based stability class (Himmelstoss et al. 2018) together with an indication of which transects change class with the extraction method.

5.4 Relative importance of tidal stage

Even on this microtidal coast, correcting for tide changed mean LRR by 0.11 - 0.45 m yr^{-1}, more than the mean influence of the extraction method at all slopes tested, because higher tides happened to fall in the later part of the record. It is often argued that tidal effects can be neglected when two methods are applied to the same images. Our results show that this holds for the difference between the methods but not for the rates themselves. The two end-point comparisons also show that the tidal effect on EPR is a matter of chance in the choice of end dates: it was almost nil for 2016 - 2026 and up to 0.63 m yr^{-1} for 2016 - 2025. The tide did not, however, significantly account for the date-to-date fluctuations in mean position, whose range of about 15 m exceeds the 3 - 13 m implied at the central point over the slopes tested. Predicted tide was also closely tied to acquisition date

within the year (r = 0.95), probably because a sun-synchronous satellite samples a tide with a strong diurnal component at a fixed local time, so selecting scenes by season also selects tidal stage. We did not examine this further, but it means that tide and season cannot be separated in this record. The main remaining uncertainty is the beach slope, which could be estimated from dense Sentinel-2 time series (Vos et al. 2020) or constrained with published beach profiles. Only astronomical tide was considered; wave set-up can affect the upper beach at Cua Dai during storms (Nguyen, Tran, and Nguyen 2021) and was not corrected here.

5.5 Drivers of shoreline change

The method-independent pattern is consistent with earlier work on this coast, although our data do not test causes directly. Previous studies attributed the erosion at Cua Dai to interaction between hard protection structures and waves and to dredging in the Thu Bon mouth (Mau, Trung, and Binh 2019), to sediment loss in the estuary together with reduced river sediment supply and mining (Hung et al. 2017), and to an erosion wave propagating under longshore transport and aggravated by seawalls (Tanaka et al. 2018). At basin scale, recent assessments report substantial riverbed incision in the Vu Gia - Thu Bon system (63.3 Mm^3 in 2010 - 2021) and attribute reductions in sediment budget to dams and sand mining, although the shares depend on how mining volumes are estimated (Nguyen et al. 2024). Against this background, significant erosion at Hoi An Tay (13.8 - 20.0% of transects) alongside frequent accretion at Hoi An Dong (50%) suggests that the sector north of the inlet has not responded uniformly, while **Fig. 4**c shows sand bodies at the inlet changing form and position through the record. Their origin cannot be determined from these shorelines alone; recovery, interventions and spit dynamics are all plausible. The inlet itself was excluded from the statistics, and its evolution is better described from the images than by a rate.

5.6 Limitations

Several limitations should be borne in mind when interpreting these results. First, in the absence of independent reference shorelines, the analysis quantifies agreement between methods rather than accuracy, and it cannot establish which method lies closer to the true waterline. The 11-date rate used as a point of comparison in Sect. 4.5 is itself one estimate and not a true rate. One scene per year cannot separate interannual change from seasonal differences between February and April, tidal stage was confounded with acquisition date, and linear regression may not suit sectors that change episodically.

FES2022 accounts for the astronomical tide only, so storm surge, wave set-up and run-up are not corrected, and each sensitivity run applied a single slope to the entire coast. The uniform 10 m DSAS uncertainty follows the accuracy published for microtidal sites (Vos et al. 2023) rather than a per-shoreline error budget. The tests relating offset to tide, date and sensor rest on 11 dates and are exploratory. Scattered landward departures of 30 - 45 m on individual transects in February 2017, seen in both datasets, have no identified cause and were retained. Finally, the exclusion of inlet sectors and of transects with multiple crossings means that the results are most representative of the open sandy coast.

6 Conclusions

Comparing pixel-based (MNDWI) and sub-pixel (SAET) shorelines from 11 Sentinel-2 scenes on 1,914 common DSAS transects along about 100 km of the Da Nang coast showed that the pixel-based line lay

systematically 4.8 - 7.6 m seaward of the sub-pixel line, about a quarter to two fifths of a 20 m SWIR1 pixel. At coast scale this offset nearly cancelled in the rates, with a mean difference of 0.07 m yr^{-1} for LRR. At transect scale it did not, because offsets correlated weakly between dates, and the limits of agreement for LRR were −0.84 to +0.70 m yr^{-1}. Using 11 dates rather than three reduced this scatter by more than a third.

At coast scale, however, both tidal correction and date selection outweighed the extraction method. Tide correction raised mean LRR by 0.11 - 0.45 m yr^{-1} over the slopes tested, and its effect on EPR depended on the tidal levels of the two end dates. Date selection had the largest effect, with three-date subsets yielding coast-mean rates from -0.60 to +1.48 m yr^{-1}. The three dates of 2016, 2020 and 2025 suggested net retreat, whereas all 11 dates gave a small positive mean rate with most transects statistically stable.

These results describe agreement between methods, not accuracy, because no independent reference shorelines were available. They suggest that DSAS assessments based on medium-resolution imagery should report signed offsets for each date, test the sensitivity of rates to tide, beach slope and date selection, and be cautious in stating a net coastal trend from few images. Denser Sentinel-2 time series with estimated beach slopes, wave data and independent reference shorelines would allow these effects to be separated and accuracy to be tested directly.

References

Amoroso PP, FG Figliomeni, C Parente (2023) A new water index proposal for coastline extraction from Landsat 9 OLI images. In: 2023 IEEE International Workshop on Metrology for the Sea (MetroSea). IEEE, pp 158 - 163. https://doi.org/10.1109/MetroSea58055.2023.10317569

Attwan MA, AHH Alboabidalah, MS Al-Zuhairy (2026) Monitoring of morphological changes and shoreline shifts using various remote sensing data: an overview. AIP Conf Proc 3379:050015. https://doi.org/10.1063/5.0306472

Aviso (2024) FES2022 (Finite Element Solution) ocean tide (ocean_tide_extrapolated). https://doi.org/10.24400/527896/A01-2024.004

Bergsma EWJ, AN Klotz, S Artigues, M Graffin, A Prenowitz, JM Delvit, R Almar (2024) Shoreliner: a sub-pixel coastal waterline extraction pipeline for multi-spectral satellite optical imagery. Remote Sens 16:2795. https://doi.org/10.3390/rs16152795

Bishop-Taylor R, S Sagar, L Lymburner, I Alam, J Sixsmith (2019) Sub-pixel waterline extraction: characterising accuracy and sensitivity to indices and spectra. Remote Sens 11:2984. https://doi.org/10.3390/rs11242984

Bland JM, DG Altman (1986) Statistical methods for assessing agreement between two methods of clinical measurement. Lancet 327:307–310. https://doi.org/10.1016/S0140-6736(86)90837-8

Boak EH, IL Turner (2005) Shoreline definition and detection: a review. J Coast Res 21:688–703. https://doi.org/10.2112/03-0071.1

Cabezas-Rabadán C, JE Pardo-Pascual, J Palomar-Vázquez, A Cooper (2025) A remote monitoring approach for coastal engineering projects. Sci Rep 15:2955. https://doi.org/10.1038/s41598-025-86485-y

Castelle B, G Masselink, T Scott, C Stokes, A Konstantinou, V Marieu, S Bujan (2021) Satellite-derived shoreline detection at a high-energy meso-macrotidal beach. Geomorphology 383:107707. https://doi.org/10.1016/j.geomorph.2021.107707

493 Castelle B, A Ritz, V Marieu, A Nicolae Lerma, M Vandenhove (2022) Primary drivers of multidecadal spatial
494 and temporal patterns of shoreline change derived from optical satellite imagery. Geomorphology
495 413:108360. https://doi.org/10.1016/j.geomorph.2022.108360
496 Chen C, S Lv, N Kong, M Li, Z Jin, X Yan, A Zhu, X Yang, J Gao (2026) A multi-stage strategy and geoscience
497 knowledge-based method for shoreline extraction from Landsat time-series. Environ Sustain Indic
498 30:101153. https://doi.org/10.1016/j.indic.2026.101153
499 Cohen J (1968) Weighted kappa: nominal scale agreement with provision for scaled disagreement or partial credit.
500 Psychol Bull 70:213–220. https://doi.org/10.1037/h0026256
501 Dervisoglu A, BB Bilgilioğlu, N Yağmur (2019) Comparison of pixel-based and object-based classification
502 methods in determination of wetland coastline. Int J Environ Geoinformatics 6:327–332.
503 https://doi.org/10.30897/ijegeo.666185
504 Dinh NQ, HN Vu, ST Ho, TV Nguyen, XT Nguyen, H Tanaka (2021) Long-term shoreline evolution using DSAS
505 technique: a case study of Quang Nam Province, Vietnam. J Mar Sci Eng 9:1124.
506 https://doi.org/10.3390/jmse9101124
507 Genz AS, CH Fletcher, RA Dunn, LN Frazer, JJ Rooney (2007) The predictive accuracy of shoreline change rate
508 methods and alongshore beach variation on Maui, Hawaii. J Coast Res 23:87–105.
509 https://doi.org/10.2112/05-0521.1
510 Himmelstoss EA, RE Henderson, MG Kratzmann, AS Farris (2018) Digital Shoreline Analysis System (DSAS)
511 version 5.0 user guide. U.S. Geological Survey, https://doi.org/10.3133/ofr20181179
512 Himmelstoss EA, RE Henderson, MG Kratzmann, AS Farris (2021) Digital Shoreline Analysis System (DSAS)
513 version 5.1 user guide. U.S. Geological Survey, https://doi.org/10.3133/ofr20211091
514 Hung NT, BT Vinh, SY Nam, JL Lee (2017) Cause analysis of erosion-induced resort washout on Cua Dai Beach,
515 Vietnam. J Coast Res SI 79:214–218. https://doi.org/10.2112/SI79-044.1
516 Künsch HR (1989) The jackknife and the bootstrap for general stationary observations. Ann Stat 17:1217–1241.
517 https://doi.org/10.1214/aos/1176347265
518 Landis JR, GG Koch (1977) The measurement of observer agreement for categorical data. Biometrics 33:159–
519 174. https://doi.org/10.2307/2529310
520 Lappe R, T Ullmann, F Bachofer (2022) State of the Vietnamese coast—assessing three decades (1986 to 2021)
521 of coastline dynamics using the Landsat archive. Remote Sens 14:2476.
522 https://doi.org/10.3390/rs14102476
523 Luijendijk A, G Hagenaars, R Ranasinghe, F Baart, G Donchyts, S Aarninkhof (2018) The state of the world's
524 beaches. Sci Rep 8:6641. https://doi.org/10.1038/s41598-018-24630-6
525 Lyard FH, DJ Allain, M Cancet, L Carrère, N Picot (2021) FES2014 global ocean tide atlas: design and
526 performance. Ocean Sci 17:615–649. https://doi.org/10.5194/os-17-615-2021
527 Mau LD, PB Trung, TV Binh (2019) Erosion features along Cua Dai beach, Hoi An city, Quang Nam province,
528 Vietnam. Vietnam J Mar Sci Technol 18:21–31. https://doi.org/10.15625/1859-3097/18/4A/13634
529 Mentaschi L, MI Vousdoukas, JF Pekel, E Voukouvalas, L Feyen (2018) Global long-term observations of coastal
530 erosion and accretion. Sci Rep 8:12876. https://doi.org/10.1038/s41598-018-30904-w

Ngo VL, VB Dang, KB Dang, CC Ngo, TPN Pham, B Burkhard, TKC Giap (2020) Assessment of shoreline changes for setback zone establishment from Son Tra (Da Nang city) to Cua Dai (Hoi An city), Vietnam. Vietnam J Earth Sci 42:363–383. https://doi.org/10.15625/0866-7187/42/4/15410

Nguyen AT, L Hens (2017) A Digital Shoreline Analysis System (DSAS) applied on mangrove shoreline changes along the Giao Thuy coastal area (Nam Dinh, Vietnam) during 2005–2014. Vietnam J Earth Sci 39:87–96. https://doi.org/10.15625/0866-7187/39/1/9231

Nguyen BQ, SA Kantoush, VB Doan, T Sumi (2024) An assessment of uncontrolled human interventions on the contemporary sediment budget and morphological alterations of the Vu Gia Thu Bon River basin, central Vietnam. Heliyon 10:e31476. https://doi.org/10.1016/j.heliyon.2024.e31476

Nguyen NT, HC Do, VU Dinh, TS Nguyen, AT Tran, DN Le (2017) Shoreline change analysis with remote sensing data in the Hau River mouth area. Vietnam J Mar Sci Technol 17:386–392. https://doi.org/10.15625/1859-3097/17/4/8858

Nguyen NT, TT Tran, TV Nguyen (2021) Study on the effects of wave-induced setup on coastal evolution of the Cua Dai beach, Hoi An. Vietnam J Mar Sci Technol 21:247–257. https://doi.org/10.15625/1859-3097/16653

Nguyen VA, TT Tran, XH Trieu (2025) Shoreline change analysis in Da Nang, Vietnam, using CoastSat: a framework for assessing algal bloom risk. Hue Univ J Sci Nat Sci 134:25–37. https://doi.org/10.26459/hueunijns.v134i1S-3.7938

Palomar-Vázquez J, JE Pardo-Pascual, J Almonacid-Caballer, C Cabezas-Rabadán (2023) Shoreline Analysis and Extraction Tool (SAET): a new tool for the automatic extraction of satellite-derived shorelines with subpixel accuracy. Remote Sens 15:3198. https://doi.org/10.3390/rs15123198

Pardo-Pascual JE, J Almonacid-Caballer, LA Ruiz, J Palomar-Vázquez (2012) Automatic extraction of shorelines from Landsat TM and ETM+ multi-temporal images with subpixel precision. Remote Sens Environ 123:1–11. https://doi.org/10.1016/j.rse.2012.02.024

Pardo-Pascual JE, E Sánchez-García, J Almonacid-Caballer, J Palomar-Vázquez, E Priego de los Santos, A Fernández-Sarría, A Balaguer-Beser (2018) Assessing the accuracy of automatically extracted shorelines on microtidal beaches from Landsat 7, Landsat 8 and Sentinel-2 imagery. Remote Sens 10:326. https://doi.org/10.3390/rs10020326

Shrout PE, JL Fleiss (1979) Intraclass correlations: uses in assessing rater reliability. Psychol Bull 86:420–428. https://doi.org/10.1037/0033-2909.86.2.420

Sun W, C Chen, W Liu, G Yang, X Meng, L Wang, K Ren (2023) Coastline extraction using remote sensing: a review. GISci Remote Sens 60:2243671. https://doi.org/10.1080/15481603.2023.2243671

Tanaka H, DV Duy, Y Mitobe, NT Viet (2018) Theory for erosion wave propagation in Cua Dai Beach, Vietnam. J Coast Res SI 85:621–625. https://doi.org/10.2112/SI85-125.1

Trinh HL, JX Lim, HT Kieu, JW Er, DSC Pang, AK Law (2026) Multisensor fusion for monitoring shorelines and coastal environments: a review and perspective with satellite imagery. IEEE J Sel Top Appl Earth Obs Remote Sens 19:10910–10935. https://doi.org/10.1109/JSTARS.2026.3674566

Vos K, MD Harley, KD Splinter, JA Simmons, IL Turner (2019) Sub-annual to multi-decadal shoreline variability from publicly available satellite imagery. Coast Eng 150:160–174. https://doi.org/10.1016/j.coastaleng.2019.04.004

Vos K, MD Harley, KD Splinter, A Walker, IL Turner (2020) Beach slopes from satellite-derived shorelines. Geophys Res Lett 47:e2020GL088365. https://doi.org/10.1029/2020GL088365

Vos K, KD Splinter, MD Harley, JA Simmons, IL Turner (2019) CoastSat: a Google Earth Engine-enabled Python toolkit to extract shorelines from publicly available satellite imagery. Environ Model Softw 122:104528. https://doi.org/10.1016/j.envsoft.2019.104528

Vos K, KD Splinter, J Palomar-Vázquez, JE Pardo-Pascual, J Almonacid-Caballer, C Cabezas-Rabadán, EC Kras, AP Luijendijk, F Calkoen, LP Almeida, D Pais, AHF Klein, Y Mao, D Harris, B Castelle, D Buscombe, S Vitousek (2023) Benchmarking satellite-derived shoreline mapping algorithms. Commun Earth Environ 4:345. https://doi.org/10.1038/s43247-023-01001-2

Vousdoukas MI, R Ranasinghe, L Mentaschi, TA Plomaritis, P Athanasiou, A Luijendijk, L Feyen (2020) Sandy coastlines under threat of erosion. Nat Clim Change 10:260–263. https://doi.org/10.1038/s41558-020-0697-0

Xu H (2006) Modification of normalised difference water index (NDWI) to enhance open water features in remotely sensed imagery. Int J Remote Sens 27:3025–3033. https://doi.org/10.1080/01431160600589179

Yadav A, BM Dodamani, GS Dwarakish (2021) Shoreline analysis using Landsat-8 satellite image. ISH J Hydraul Eng 27:347–355. https://doi.org/10.1080/09715010.2018.1556569

Yulianto F, D Kushardono, S Budhiman, G Nugroho, GA Chulafak, EK Dewi, AI Pambudi (2022) Evaluation of the threshold for an improved surface water extraction index using optical remote sensing data. Sci World J 2022:4894929. https://doi.org/10.1155/2022/4894929